LIDAR-Derived National Shoreline: Empirical and Stochastic Uncertainty Analyses

Author(s): Stephen A. White, Christopher E. Parrish, Brian R. Calder, Shachak Pe'eri, and Yuri Rzhanov
Source: Journal of Coastal Research, Number 10062:62-74. 2011.
Published By: Coastal Education and Research Foundation
DOI: 10.2112/SI_62_7
URL: http://www.bioone.org/doi/full/10.2112/SI_62_7

Journal of Coastal Research	SI	62	62–74	West Palm Beach, Florida	Spring 2011

LIDAR-Derived National Shoreline: Empirical and Stochastic Uncertainty Analyses

Stephen A. White[†]*, Christopher E. Parrish[†], Brian R. Calder[‡], Shachak Pe'eri[‡], and Yuri Rzhanov[‡]

[†]NGS Remote Sensing Division
National Oceanic and Atmospheric Administration/National Ocean Service
National Geodetic Survey
Silver Spring, MD 20910, U.S.A.
Stephen.A.White@noaa.gov

[‡]Center for Coastal and Ocean Mapping
University of New Hampshire
Durham, NH 03824, U.S.A.

www.cerf-jcr.org

ABSTRACT

WHITE, S.A.; PARRISH, C.E.; CALDER, B.R.; PE'ERI, S., and RZHANOV, Y., 2011. LIDAR-derived national shoreline: empirical and stochastic uncertainty analyses. *In:* Pe'eri, S. and Long, B. (eds.), *Applied LIDAR Techniques*, Journal of Coastal Research, Special Issue No. 62, 62–74. West Palm Beach (Florida), ISSN 0749-0208.

The National Oceanic and Atmospheric Administration's (NOAA) National Geodetic Survey (NGS) is mandated to map the national shoreline, which is depicted on NOAA nautical charts, serves as an important source in determining territorial limits, and is widely used in various coastal science and management applications. The National Geodetic Survey's primary method of mapping the national shoreline is through stereo compilation from tide-coordinated aerial photography. However, over the past decade, NGS has conducted several phases of research to develop, test, and refine light detection and ranging (LIDAR)–based shoreline mapping procedures. Although important, reliable estimates of uncertainty of these products have, unfortunately, lagged behind in development. We attempt here to outline possible solutions to this lack. Specifically, this study presents and compares two new methods of assessing the uncertainty of NGS' LIDAR-derived shoreline: an empirical (ground-based) approach and a stochastic (Monte Carlo) approach. We observe uncertainties in the horizontal position of the shorelines on the order of 1 to 6 m (95%) depending on location and, especially, beach slope. We show that appropriate adjustment for biases can reduce these to about 1 m (95%) and that the two methods of assessing the uncertainty show good agreement in our test cases.

ADDITIONAL INDEX WORDS: *National shoreline, topographic LIDAR, uncertainty, Monte Carlo simulation, empirical measurements, stochastic modeling.*

INTRODUCTION

The National Geodetic Survey (NGS), a program office of the National Oceanic and Atmospheric Administration's (NOAA's) National Ocean Service (NOS), maintains a Coastal Mapping Program with the goal of providing accurate, consistent, and up-to-date national shoreline for the United States and its territories. NGS and its predecessors have been conducting shoreline mapping activities since the original "Survey of the Coast" in 1807 (Shalowitz, 1964), and the shoreline depicted on NOS nautical charts is treated as the legal shoreline by many U.S. agencies (Graham, Sault, and Bailey, 2003). In addition to its primary use on nautical charts to assist in safe navigation, this national shoreline serves numerous other purposes, ranging from determination of legal boundaries to coastal management and environmental applications, *e.g.,* climate change studies (Morton, Miller, and Moore, 2004; Scavia *et al.,* 2002; Titus and Richman, 2001).

However, in keeping with current developments in hydrographic mapping practice (*e.g.,* IHO, 2008), development of shoreline position estimates are insufficient: to quantify the measurements, estimates of the uncertainty are essential. These estimates are included in metadata to inform the construction of products from the data and as a means to guide decision-making processes within the Coastal Mapping Program.

Methods for deriving uncertainty estimates have lagged behind the ability to generate shorelines by newer technologies such as light detection and ranging (LIDAR). We propose here two methods to approach this difficulty. First, we describe a field survey technique that provides estimates of uncertainty based on observations with high-precision integrated GPS and laser-level systems. While extremely accurate, this method is time consuming and requires significant investment of human and technological resources, making it infeasible for large-scale deployment. We therefore also propose a scheme based on stochastic simulation of the product construction process that allows us to estimate what the plausible variation of the observed product shoreline might be, given what we know about the observations that are used to derive it.

We examine and compare the behavior of these schemes, using data collected over the North Carolina Outer Banks in

DOI:10.2112/SI_62_7 received and accepted in revision 13 September 2010.

the vicinity of Cape Hatteras. Using the field-based estimation technique to ground-truth uncertainty, we then compare the behavior of our Monte Carlo–based simulation technique and show that the results would lead us to the same conclusions about the data, irrespective of method. We consider also the practicality of the methods and the caveats that we might apply to their future development and utilization. We conclude with recommendations for future research aimed at more rigorous uncertainty models for the LIDAR-derived national shoreline.

Background: NGS Shoreline Definition and Photogrammetric Mapping Procedures

Universally accepted methodologies and definitions for a standard shoreline do not exist. Indeed, numerous indicators or proxies for shoreline position have been used in shoreline mapping and described in the literature, including vegetation lines; dune lines; dune toes; bluff or cliff lines; beach scarps; berm crests; the high water line (HWL), interpreted as the wet–dry line from the last high tide; and coastal structures, such as seawalls or bulkheads—in addition to datum-based shorelines (Boak and Turner, 2005; Crowell, Leatherman, and Buckley, 1991; Leatherman, 2003; Moore, 2000; Moore, Ruggiero, and List, 2006; Morton, 1991; Morton and Speed, 1998; Pajak and Leatherman, 2002). While comparisons of these different shoreline indicators or proxies and of different shoreline mapping techniques are interesting and important, they are outside the scope of the present study: we limit our focus here to the national shoreline and, therefore, to NGS's specific shoreline definition and mapping procedures. (Similar techniques could be used to assess shorelines defined using other methods.)

Historically, the shoreline depicted on NOS topographic sheets (T-sheets) was an interpreted high water line (Boak and Turner, 2005; Moore, Ruggiero, and List, 2006; NRC, 2004). After the 1930s, the component of the U.S. Coast and Geodetic Survey that later became the NOS/NGS Remote Sensing Division adopted procedures for shoreline mapping from tide-coordinated aerial photography (Smith, 1981). The current procedures are designed to produce lines representing the intersection of the land (at the specific time of data acquisition) and the water surfaces of the mean high water (MHW) and mean lower low water (MLLW) tidal datums (NRC, 2004). These procedures entail compiling the land–water interface in stereo photography flown within a time window calculated from the predicted or observed (*via* water level stations) time of MHW or MLLW plus or minus a specified vertical tolerance, which is a function of the tidal range (Graham, Sault, and Bailey, 2003). Near-infrared (NIR) emulsion or the NIR band in imagery from a multispectral digital camera is used, along with a suitable long-wave-pass optical filter, to create sharp contrast between land and water in the imagery, enabling the human compiler to more easily and accurately delineate the land–water interface in the tide-coordinated aerial photography (Parrish *et al.,* 2005). The uncertainty of the shoreline mapped through these procedures is a function of several variables, including the water level tolerance (*i.e.,* the amount by which, according to NGS policy, the observed or predicted water level at the time of aerial image acquisition can be above or below MHW or MLLW), and uncertainty in the water level observations or predictions, photogrammetric aerotriangulation, and the manual compilation process, which, in turn, can be affected by wave runup.

NGS LIDAR Shoreline Mapping

While the photogrammetric procedures remain NGS's primary methodology for mapping the national shoreline, over the course of the past decade NGS has worked with numerous partners to develop, test, and refine new airborne LIDAR shoreline mapping procedures. One of the main benefits of using LIDAR is that the tide-coordination requirements are not as stringent as with the photogrammetric procedure: it is typically only necessary to acquire the data below a certain stage of the tide, rather than within a narrow tide window. Thus, the efficiency of data acquisition is increased greatly. Furthermore, the LIDAR-based procedures assist in eliminating some of the subjectivity associated with the manual photogrammetric compilation methods and in providing multiuse data that can benefit other coastal projects and programs (Scott, Wijekoon, and White, 2009; White, 2007). The specific methods used by NGS in mapping the national shoreline using LIDAR are described in the following section. Related methods of LIDAR shoreline mapping are also discussed in Liu, Sherman, and Gu (2007), Robertson *et al.* (2004), and Stockdon *et al.* (2002).

LIDAR SHORELINE MAPPING WORKFLOW

NGS's LIDAR shoreline mapping procedures are illustrated graphically in the workflow diagram of Figure 1. Typically, in LIDAR acquisition for shoreline mapping, NGS specifies a required point spacing of approximately 1 m in both the along- and across-track directions. The resulting laser measurements are received as a point cloud in LAS format (ASPRS, 2009) that is referenced to the geodetic frame NAD 83 (CORS96) (Snay and Soler, 2008). The LIDAR point cloud is cleaned by removing outliers, including LIDAR returns from birds, atmospheric particles, and electronic noise in the receiver. Automatic and manual methods are used to identify potentially erroneous measurements, with automatic parameters adjusted for the environment and manual assessments supported by high-resolution aerial photography. The manual inspection of the data is primarily used to verify performance of the automatic methods. If the LIDAR data will be used solely for shoreline mapping, significant time can be saved in this step by limiting the data cleaning to a narrow swath encompassing the shoreline.

The NAD83 (CORS96) ellipsoid heights of the edited data are transformed to MHW using NOAA's vertical datum transformation utility, VDatum (Myers *et al.,* 2007). Within the VDatum software, the LIDAR data are first transformed from ellipsoidal NAD83 (CORS96) heights to orthometric North American Vertical Datum of 1988 (NAVD88) heights using NGS's current hybrid geoid model, GEOID09. The software then transforms the LIDAR elevations from

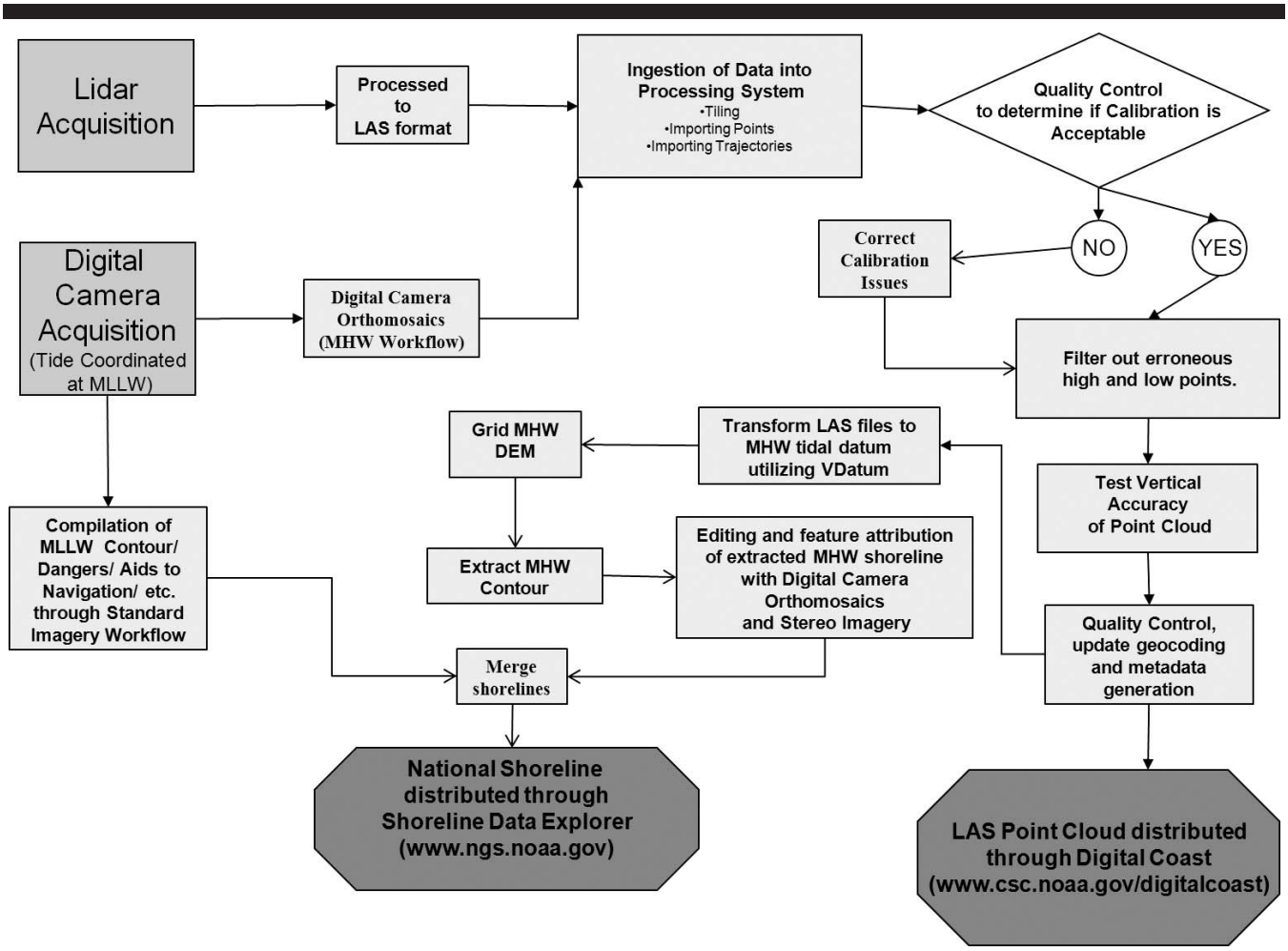

Figure 1. NGS's LIDAR shoreline mapping procedures.

NAVD88 to local mean sea level through modeled topography of the sea surface (TSS) grids and, finally, to MHW using gridded tidal datum fields. Tide models are derived from hydrodynamic circulation models driven by coastal observations (Parker, 2002) and corrected by observed errors at tide gauges using NOAA's tidal constituent and residual interpolation (TCARI) method (Hess, 2002). Estimated uncertainties in the datum realizations and datum transformations supported by VDatum are currently published on NOAA's VDatum website (NOAA, 2009).

After transformation to MHW, the LIDAR data are interpolated onto a regular 1.5-m grid *via* a triangulated irregular network (TIN) constructed through Delauney triangulation with the constraint that no triangle with a side length over 3 m is allowed. The 0-m MHW contour is then extracted from the grid by linear interpolation. Finally, the extracted shoreline is inspected and attributed using aerial imagery to generate the product shoreline. The process outlined here and illustrated graphically in Figure 1 is further described in White (2007).

EMPIRICAL UNCERTAINTY ANALYSIS

Experiment

In spring 2008, an airborne topographic LIDAR survey was conducted along the North Carolina Outer Banks (from Ocracoke Island north to Cape Henry, Virginia) as part of NOAA's integrated ocean and coastal mapping (IOCM) initiative (Scott, Wijekoon, and White, 2009). Three test sites were selected to assess the accuracy of the LIDAR-derived MHW shorelines: Duck, Coquina Beach, and Frisco, North Carolina (Figure 2). These sites can be characterized as open coast sandy beaches, with the Duck and Coquina sites facing easterly and the Frisco site facing southerly. The slope of the beaches ranges from approximately 2° (Frisco and Coquina) to almost 5° (Duck). A few jetties, groins, detached break waters, and piers can be found along the project extents.

The survey was conducted with an Optech airborne LIDAR topographic mapper (ALTM) 3100 LIDAR system, and an Applanix medium-format digital sensor system (DSS) 439 DualCam, installed onboard a NOAA Cessna Citation. The

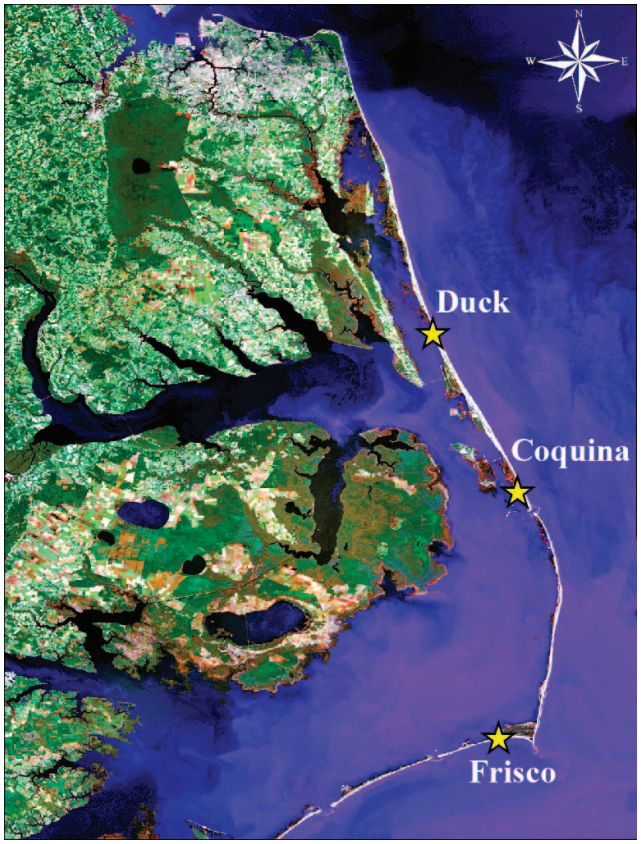

Figure 2. The three study sites for assessing the horizontal positional accuracy of LIDAR-derived MHW shorelines.

Optech ALTM 3100 LIDAR system collects data at pulse repetition frequencies (PRFs) of up to 100 kHz using a 1064-nm laser, while the DSS DualCam comprises two medium-format digital cameras, each with a 5412 × 7216 pixel charge-coupled device array capable of providing high-resolution digital orthorectified imagery. An Applanix POS-AV 510 system enabled accurate georeferencing. Each sensor was equipped with its own inertial measurement unit (IMU), while a single aircraft GPS dual-frequency antenna was used for both. The GPS signal was split two ways to accommodate the two sensors. The survey used CORS GPS base stations (Snay and Soler, 2008) in a differential mode with the onboard GPS to derive the trajectory of the aircraft.

The DSS DualCam was set to acquire natural color (400–700 nm, separated into blue, green, and red spectral bands *via* a Bayer filter) and NIR imagery (860–1100 nm), with each camera using a 60-mm focal length lens. The data were acquired at a nominal flying height of 1375 m and at a flying speed ranging from 65 to 85 m/s, resulting in a 0.16-m ground sample distance (GSD) for the imagery. Orthorectified mosaics of the DSS imagery were created with a 0.5 m GSD. The ALTM 3100 LIDAR was configured to acquire data at a PRF of 70 kHz, with a scan angle of ±16° and a scan rate of 41 Hz. At the flying height and speed listed previously, these settings yielded a LIDAR point spacing of approximately 1.25 m.

Table 1. *NOAA benchmarks and tide stations used to control the vertical positions of the shoreline transects.*

Accuracy Site	Tide Station	Vertical Benchmark ID	No. Transects
Duck	8651370	FW0686	20
Coquina	8652587	EX0141	12
Frisco	8654400	EX0249	25

Field work was performed concurrently with the airborne surveys and consisted of using geodetic-quality GPS receivers to compute coordinates on control points within the study sites' bounds to assess the vertical accuracy of the LIDAR dataset. The GPS checkpoints were collected in flat, open areas. In addition, shoreline transects were collected perpendicular to the shoreline at spacing of about 10 m with a Topcon Laser-Zone integrated laser level and real-time GPS system at all three sites.

The Topcon system used a laser level to measure millimeter-level-precision relative elevation differences along each transect extended from local tidal benchmarks. The horizontal NAD83 (CORS96) positioning was computed at the centimeter level using the real-time kinematic (RTK) GPS component of the system. Information on the benchmarks and tide stations used to control the vertical positions of the shoreline transects are provided in Table 1. The horizontal network accuracy of the benchmarks used is 0.011 m or better. For purposes of this study, the tidal datum elevation information on these benchmarks is assumed to be perfectly known (*i.e.,* to have zero uncertainty), since the tidal datum computations calculated at these locations use 19 years of data spanning an entire national tidal datum epoch, as well as differential leveling, providing internal consistencies of better than 0.009 m between benchmarks and the tide station.

Methods

For purposes of the accuracy assessment, LIDAR and GPS datasets were referenced to NAD83 (CORS96) and not converted to a tidal datum to avoid introducing datum transformation uncertainties into the assessment. The assessment of vertical accuracy was computed for the overall dataset with a combination of 62 GPS-derived checkpoints and 1025 data points derived from the Topcon system (Table 2). The overall vertical root-mean-square error ($RMSE_v$) for all sites is 0.12 m, with small variations among the sites.

The quantitative assessment of shoreline positional accuracy was conducted by interpolating the Topcon Laser-Zone transect values to determine the zero-crossing point and then computing the spatial (Euclidean) distance from this point to a point on the LIDAR-derived shoreline vector (either along the transect or to the closest point on the shoreline in Euclidean distance). Linear and cubic spline (Press *et al.,* 1992) interpolations were used to test sensitivity to interpolation methods; the methods differ in that, in addition to generating a generally smoother interpolate, cubic spline

Table 2. *LIDAR point cloud vertical accuracy statistics in units of meters.**

	Frisco	Coquina	Duck	Overall
Mean dV	−0.15	−0.08	0.03	−0.05
Minimum dV	−0.31	−0.20	−0.32	−0.54
Maximum dV	0.34	0.09	0.23	0.55
Average magnitude	0.15	0.08	0.06	0.10
Root-mean-square error	0.16	0.09	0.08	0.12
Standard deviation	0.05	0.05	0.07	0.11

* Frisco, Coquina, and Duck were calculated using data only from the Topcon system, while overall statistics were computed using GPS control, as well as data from the Topcon system.
dV = vertical difference.

methods use all available data, rather than just points adjacent to the zero-crossing location. Figure 3 shows an example of the interpolated MHW zero location (denoted by the asterisk) along a particular transect (left) and a comparison of the LIDAR-derived shoreline with numerous MHW ground-truth locations (denoted by small yellow triangles) obtained in this manner (right).

Results

As noted earlier, we assessed the horizontal discrepancy between the LIDAR-derived shoreline and the MHW ground-truth locations by two methods: (1) measurement along the transect and (2) measurement to the point on the shoreline nearest in Euclidean distance to the truth location. The comparison of methods allowed us to assess any potential difficulty due to the discretely sampled nature of the transects and shorelines. Results are shown in Tables 3 and 4. As can be seen from the tables, the choice of interpolation strategy (linear *vs.* cubic spline) has negligible effect on the results. This fact can be further understood through the graph on the left-hand side of Figure 3. This transect can be viewed as a two-dimensional cross-section of the beach profile at a particular location. We see considerable curvature to the beach face over the length of the entire transect, but because the distance between adjacent survey points along the transect was kept small (~5 m), there is little curvature between adjacent points. Hence, any reasonable interpolation strategy should produce nearly identical results. Similarly, the differences between distance measurement methods (along the transect *vs.* shortest Euclidean distance) are also seen to be negligible. However, there are distinct differences among the values for the three sites, corresponding to vertical biases observed in the data, as well as the physical characteristics of the beach in each of the three areas. Measurements for all sites were combined to give the overall assessment of the accuracy of the method (Table 5).

Horizontal Bias Correction

Differences between horizontal accuracies at the different LIDAR-derived shoreline sites appear to be primarily attributable to GPS baseline distances and the beach slope at the sites. The CORS GPS station at the Duck Field Research Facility was used as the base station in computing the postprocessed aircraft GPS trajectories. (Other CORS stations were available in or around the project area but were found to have missing data for some portions of the project, to yield poor-quality trajectories, or both; thus, for consistency, the Duck station was used exclusively in the postprocessing.) Therefore, at the Duck site, the baseline vector length from GPS base station to aircraft was considered 0 km, while at Coquina the baseline was 46 km and at the Frisco site it was 108 km. In general, the longer the baseline, the less accurate the GPS solution, leading to a less accurate derived LIDAR point cloud, since errors in the GPS trajectory propagate directly to errors in the spatial coordinates of points in the LIDAR point cloud (Baltsavias, 1999). This general rule is consistent with the larger observed vertical biases at the Coquina and Frisco sites that shift the derived shoreline landward of the MHW truth locations. Table 2 illustrates this with vertical biases of 0.03 m at Duck, −0.08 m at Coquina, and −0.15 m at the Frisco site. While the RMSE values between Duck and Coquina differ by only 0.01 m, the discrepancy in slope is relatively large (Table 6). (The slopes for the three sites were computed using the LIDAR data. This included calculating the average slope along the MHW line and the average slope for the entire beach from the land–water interface up to the toe of the dune line.) Two sites that have a similar vertical accuracy for the point clouds can have different horizontal uncertainties for a derived shoreline. This can occur if one of the datasets has a larger bias, the sites have different slope for the beach face, or both: a greater-sloping beach, such as the Duck site, provides smaller horizontal uncertainties in relation to that of a lower-sloping beach, such as the Coquina site.

A propagated horizontal bias due to the LIDAR's vertical bias was calculated for each site based on the slope of the beach at each site along the LIDAR-derived MHW line (Table 7; *cf.* Table 3). The calculation was performed as follows:

$$\Delta x = \frac{1}{\tan\theta}\Delta z_{\text{lidar bias}}, \quad (1)$$

Table 3. *Horizontal positional LIDAR-derived shoreline accuracy statistics (in meters) computed along the shoreline transects.*

	Frisco		Coquina		Duck	
	Cubic Spline	Linear	Cubic Spline	Linear	Cubic Spline	Linear
$RMSE_{HOR}$	3.59	3.63	2.18	2.16	0.53	0.56
Mean distance between LIDAR-derived MHW and Topcon-measured transects	3.55	3.58	2.12	2.10	0.45	0.50
Standard deviation of distance between LIDAR-derived MHW and Topcon-measured transects	0.56	0.58	0.54	0.54	0.29	0.27
NSSDA Accuracy$_r$ (95% CI)	5.86	5.93	3.39	3.38	0.92	0.97

Table 4. *Horizontal positional LIDAR-derived shoreline accuracy statistics (in meters) computed from the MHW tidal datum zero truth location to the closest position on the LIDAR-derived shoreline.*

	Frisco		Coquina		Duck	
	Cubic Spline	Linear	Cubic Spline	Linear	Cubic Spline	Linear
$RMSE_{HOR}$	3.60	3.62	2.19	2.18	0.53	0.55
Mean distance between LIDAR-derived MHW and Topcon-measured transects	3.56	3.58	2.13	2.12	0.46	0.47
Standard deviation of distance between LIDAR-derived MHW and Topcon-measured transects	0.55	0.57	0.51	0.53	0.28	0.29
$NSSDA\ Accuracy_r$ (95% CI)	5.71	5.73	3.79	3.77	0.92	0.95

where θ is the beach slope (assumed to be constant over short distances). Here, Δ is used to denote a bias or systematic error, as opposed to a random error. The horizontal bias estimates using Equation (1) are 0.29 m at the Duck site, −3.0 m at the Coquina site, and −4.3 m at the Frisco site. These horizontal bias estimates agree with the measured horizontal biases (*i.e.,* the average measured distances between the LIDAR-derived contour and the Topcon Laser-Zone transect MHW intersect points, presented in the empirical accuracy assessment) to within 0.21 m at the Duck site, 0.90 m at the Coquina site, and 0.75 m at the Frisco site. This, in turn, provides strong indication that the horizontal biases dominating the $RMSE_{HOR}$ values presented in Tables 3–5 are primarily attributable to vertical bias in the LIDAR data and the beach slope in each of the three sites. Table 7 presents the results with these biases removed.

STOCHASTIC ASSESSMENT OF HORIZONTAL UNCERTAINTY

Method

To provide a comparison for the empirical estimate of the uncertainty of the shoreline, and to outline a method to extend the analysis to regions where fieldwork cannot physically or economically be executed, we develop here a predictive statistical model of likely uncertainty. Where there is good knowledge of the method by which raw measurements are turned into products, and these algorithms are relatively simple (or amenable to reasonable simplifying assumptions), analytical methods of uncertainty propagation may be used for this. (In multibeam sonar, *e.g.,* this has been the case for a number of years; see Calder and Mayer, 2003; Hare, Godin, and Mayer, 1995; and the references therein.) In the case of the derived shoreline, however, the construction method is complex and nonlinear (Figure 1). Consequently, although we could in theory construct uncertainty estimates for the elevation measurements by formal methods, it would be mathematically difficult to propagate these into estimates of the horizontal uncertainty of the shoreline without making limiting assumptions. In a similar way, given that we have to adopt a sampler-based approach to the estimation of uncertainty to make any progress, it is simpler, with fewer assumptions, to sample on the raw measurements generated by the LIDAR—where we have some idea as to the plausible distributions of the variables of interest—than to attempt to compute formally propagated uncertainties for the elevations and then sample from assumed distributions that might not

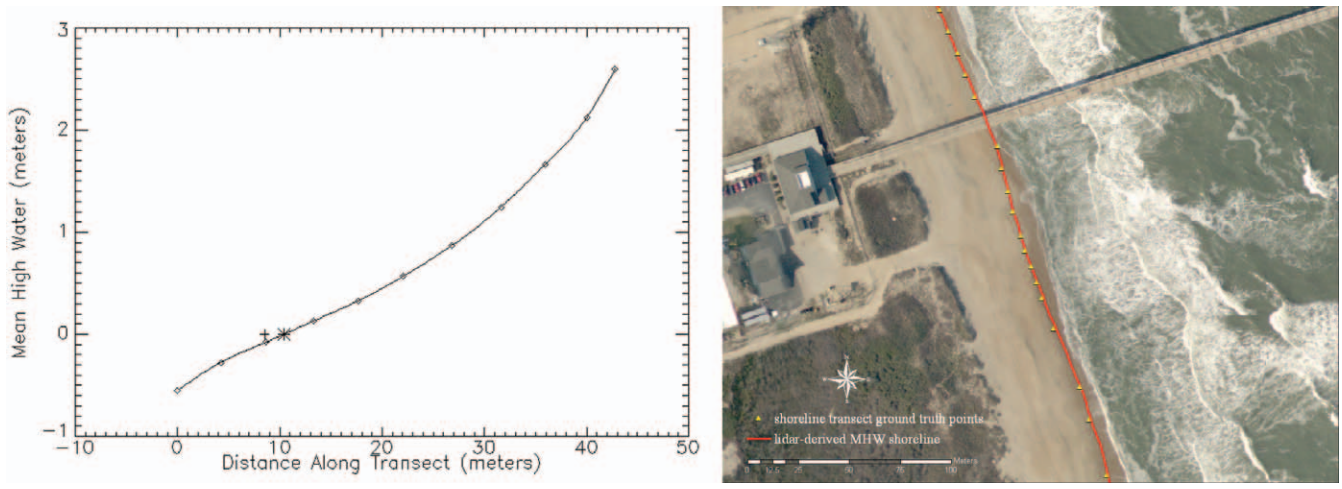

Figure 3. (Left) Example of a transect from the Duck study site surveyed with the integrated laser level RTK GPS system. Each small diamond denotes a surveyed location (with accurate three-dimensional coordinates) along the transect. The asterisk (*) denotes the interpolated position of the MHW zero crossing on this transect, and the plus sign (+) denotes the closest point on the LIDAR-derived MHW shoreline. (Right) The LIDAR-derived shoreline (red vector) with numerous MHW truth locations (yellow triangles) overlaid. Each yellow triangle represents the MHW ground-truth location along a particular transect obtained through the procedure depicted on the left.

Table 5. *Combined horizontal positional LIDAR-derived shoreline accuracy statistics (in meters) computed for all accuracy sites.*

	Along Transect		Nearest Position	
	Cubic Spline	Linear	Cubic Spline	Linear
$RMSE_{HOR}$	2.60	2.62	2.61	2.62
Mean distance between LIDAR-derived MHW and Topcon-measured transects	2.16	2.19	2.17	2.18
Standard deviation of distance between LIDAR-derived MHW and Topcon-measured transects	1.46	1.46	1.46	1.46
NSSDA $Accuracy_r$ (95% CI)	4.50	4.44	4.51	4.53

adequately reflect the behavior of the variates due to the underlying measurements (compare, *e.g.,* Liu, Sherman, and Gu, 2007). Adopting a Monte Carlo approach at the raw measurements makes the fewest assumptions, automatically incorporates all correlations and physical constraints on the data, and is not significantly more computationally complex than the alternatives.

The outline of the method is given in Figure 4. We first back-project the resolved elevations from the trial dataset through the laser geolocation equation (Filin, 2001; Lindenberger, 1989; Parrish, 2007; Vaughn *et al.,* 1996) to determine the indicated range and angles resolved by the LIDAR during flight. (The high-resolution position and attitude were derived directly from the output of the positioning and orientation system data, which are recorded at 200 Hz.) We then model the potential uncertainties of positioning, attitude measurement, range, and angle determination to form, from the "true" data, a series of "plausible" estimates of the variables of interest that form, in effect, an ensemble of possible observed datasets. These are then processed through all of the normal geolocation, digital terrain model DTM construction, and shoreline extraction code as if they were true observed datasets, and an ensemble of shorelines is constructed. The "true" dataset is processed through the same analysis to ensure consistency, and the resulting shoreline estimate is then compared directly to the plausible ensemble to estimate the product uncertainty of the shoreline—the primary estimate of interest.

The uncertainty model used to produce the ensemble of plausible datasets is the key to obtaining realistic estimates of uncertainty at the end of the process. In these experiments, we have assumed that the measurements of interest have been gathered over a short period; therefore, it is appropriate to model the positional uncertainty as a combination of a static offset corresponding to the GPS's constellation uncertainty, determined once for the entire dataset, and a (significantly smaller) uncertainty corresponding to random variation of the position solution generated by the flight IMU, which varies with each shotpoint. (Baseline effects as outlined earlier would be included in the GPS static offset uncertainty component if they were suspected to be significant at the site of interest.) We treat all three dimensions equally since they have similar properties when resolved with either RTK or postprocessed kinematic (PPK) GPS techniques (the analysis here uses the latter techniques). We model attitude uncertainty as uncorrelated Gaussian random variables of fixed variance and zero mean and treat the range estimated using the same method, accumulating a number of terms relating to time uncertainty and drift (Balstavias, 1999; Habib *et al.,* 2008; Morin, 2002) into one term for simplicity (and lack of such detailed information from the LIDAR manufacturer). Finally, we model the angle measured as a combination of a Gaussian component with fixed variance to represent measurement uncertainty and a component with variance dependent on the angle measured to represent potential for torsion on the beam connecting the scan mirror and the measurement reflector target (Morin, 2002). The calibration constants are given in Table 8 and are derived primarily from Morin (2002) and Baltsavias (1999), with updates for the particular system under test estimated from the ground-control software (alignment angles) and manufacturer data (measurement uncertainties). Many other models are possible, and there has been much research (Balstavias, 1999; Habib *et al.,* 2008; Morin, 2002) into possible alternatives. We believe that this model provides a suitable working base for preliminary analysis without overcomplicating the generation process or requiring many parameters that are either difficult to compute or require more detailed knowledge of the LIDAR than most manufacturers are willing to provide.

Table 6. *Slope (in degrees) of the beaches at the shoreline accuracy assessment sites.*

	Frisco	Coquina	Duck
Mean MHW line	2.00	1.53	5.87
Mean for entire beach	2.23	2.15	4.67

Results

After processing, each shoreline is represented by a piecewise parametric curve in two dimensions, $[x(t), y(t)]^T = \Lambda_{(0 \le t < 1)}[\{x_i, y_i\}, 1 \le i \le N]$, where $\Lambda_{(X)}(S)$ indicates appropriate interpolation of set S on range X. We assess the offset between each contour in the ensemble and the reference shoreline by computing the unit normal to the reference shoreline, $\tilde{n}$, at N_T equispaced points along the curve, $[x_R(t_i), y_R(t_i)]^T$, $t_i = i/N_T$, $0 \le i < N_T$, through a second-order central-difference estimate of the tangent to the curve and then solving for the intersection of the normal line and ensemble curve (if such intersection exists). We then accumulate statistics of the orthogonal distance from the reference shoreline to the ensemble shorelines along the normal at each test point as a summary of the horizontal shift of the members of the ensemble and therefore of the

Table 7. *Horizontal positional shoreline accuracy statistics (in meters) computed along the shoreline Topcon transects, with systematic biases removed.*

	Frisco		Coquina		Duck	
	Cubic Spline	Linear	Cubic Spline	Linear	Cubic Spline	Linear
$RMSE_{HOR}$	0.36	0.36	0.43	0.47	0.54	0.55
Mean distance between LIDAR-derived MHW and Topcon-measured transects	0.32	0.32	0.39	0.43	0.44	0.48
Standard deviation of distance between LIDAR-derived MHW and Topcon-measured transects	0.16	0.17	0.17	0.19	0.32	0.28
NSSDA accuracy (95% circular error)	0.60	0.63	0.74	0.81	0.93	0.93

horizontal uncertainty of the product shoreline under test. In this preliminary assessment of the method, the data from the Duck test site were used.

The distributions of orthogonal offsets about the reference shoreline can be determined directly from the ensemble (Figure 5; we have shown only four representative sections, although this can be done everywhere along the reference shoreline.) The data mostly show a central tendency and approximately symmetric distribution about the reference shoreline (although heavier than Normal tails are typically observed), with an obvious exception about $t \approx 0.46$, which corresponds to the area around the pier at Duck, where we have removed the outer section of the pier from consideration during shoreline extraction and patched together the shoreline around the remainder. This is, essentially, an artifact of the processing in this case, and in normal practice the entirety of the pier structure would be removed from consideration during preprocessing of the data and the shoreline would be patched up with an appropriately smooth transition corresponding to the surface beneath the pier. (Alternative processing methods are also used, depending on the expected usage of the data.) While this effect illustrates the difficulties that anthropogenic structures pose to this type of automated analysis, a much larger topic than it is possible to address here, we treat this particular circumstance by censoring these test points in the remainder of the analysis results.

A summary estimate of the uncertainty of the shoreline can be constructed by considering an appropriate confidence interval (CI) on the orthogonal offsets at each of the $N_T = 100$ test points. We computed a theoretical estimate of the 95% CI by estimating the standard deviation of the

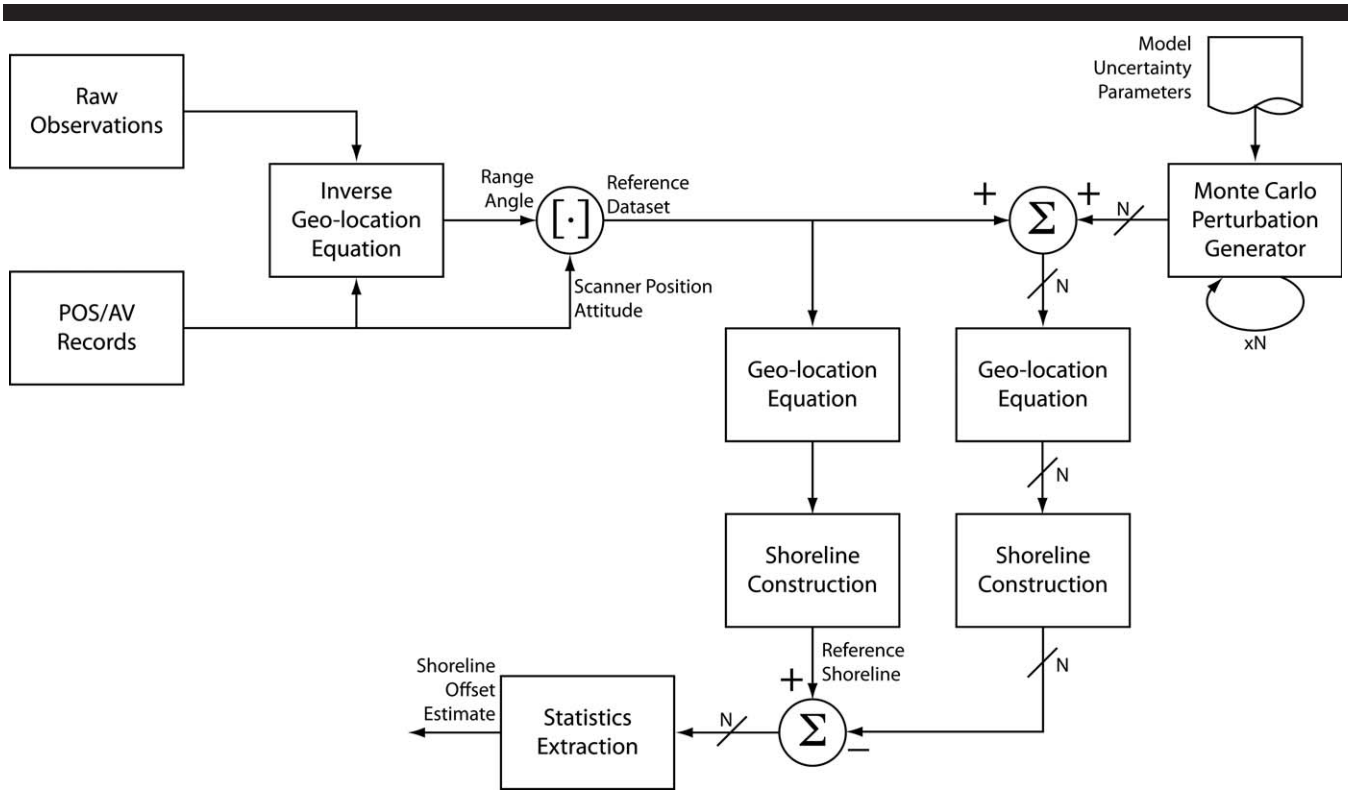

Figure 4. Configuration of the Monte Carlo analysis method for determining horizontal uncertainty of the shoreline. Replicating the processing method used for standard datasets ensures that the complexity of the method is represented in the uncertainty estimate.

Table 8. *Uncertainty parameters for the Monte Carlo module.**

Variable	Value
XYZ offsets	50 mm
Roll offset	0.0006°
Pitch offset	0.0006°
Heading offset	0.0012°
GPS absolute	80 mm
GPS relative	10 mm
Roll measurement	0.003°
Pitch measurement	0.003°
Heading measurement	0.004°
Range measurement	50 mm
Angle measurement	0.001°
Refraction angle	0.0011°
Latency angle	0.005°
Torsion coefficient	7.3614×10^{-5}

* All values are reported at one standard deviation.

orthogonal offsets (and then scaling, assuming a Gaussian distribution, which, as seen from the histogram in Figure 5, is a reasonable but not a perfect model). We also computed an empirical highest-density region estimate of the 95% CI by computing the 2.5% and 97.5% quantiles from the empirical cumulative density function of the offsets. The results (Figure 6) are broadly similar within the limits of estimation accuracy imposed by the number of members in the Monte Carlo ensemble. This suggests that the effective horizontal displacement of the data is approximately 1.0 m (95%) at the southern end of the shoreline, rises to approximately 3.3 m (95%) immediately after the pier region, and then drops back to approximately 1.5 m (95%) toward the northern end of the beach. These results are similar to the estimates conducted during the field trials, although a little more conservative in places. (The variations along the shoreline are strongly correlated with the local slope of the beach, a subject to which we return in Discussion.) This corresponds well with the relatively conservative assessment of component uncertainties in the Monte Carlo model for the raw measurements of the LIDAR and the simplified model of uncertainty construction that was used in this test. A spatial interpretation of the uncertainty of the reference shoreline is shown in Figure 7 for both estimates. The offset of the outer 95% CI curves has been exaggerated 20 times so that the curves are visible on the scale of the entire shoreline.

Discussion

The empirical (field survey) approach used in this study to assess the positional uncertainty of the LIDAR-derived shoreline was shown to work reliably. Observed benefits of the approach include the following:

(1) The integrated laser level–RTK GPS technology lends itself well to this type of accuracy assessment in that it is possible to quickly obtain high-accuracy, three-dimensional spatial coordinates and tidally referenced heights along numerous shoreline transects.
(2) By running the transects from a tidal benchmark, we obtain an independent set of reference points along the intersection of the tidal datum and beach profile. Specifically, the reference data are free from any uncertainty associated with vertical datum transforma-

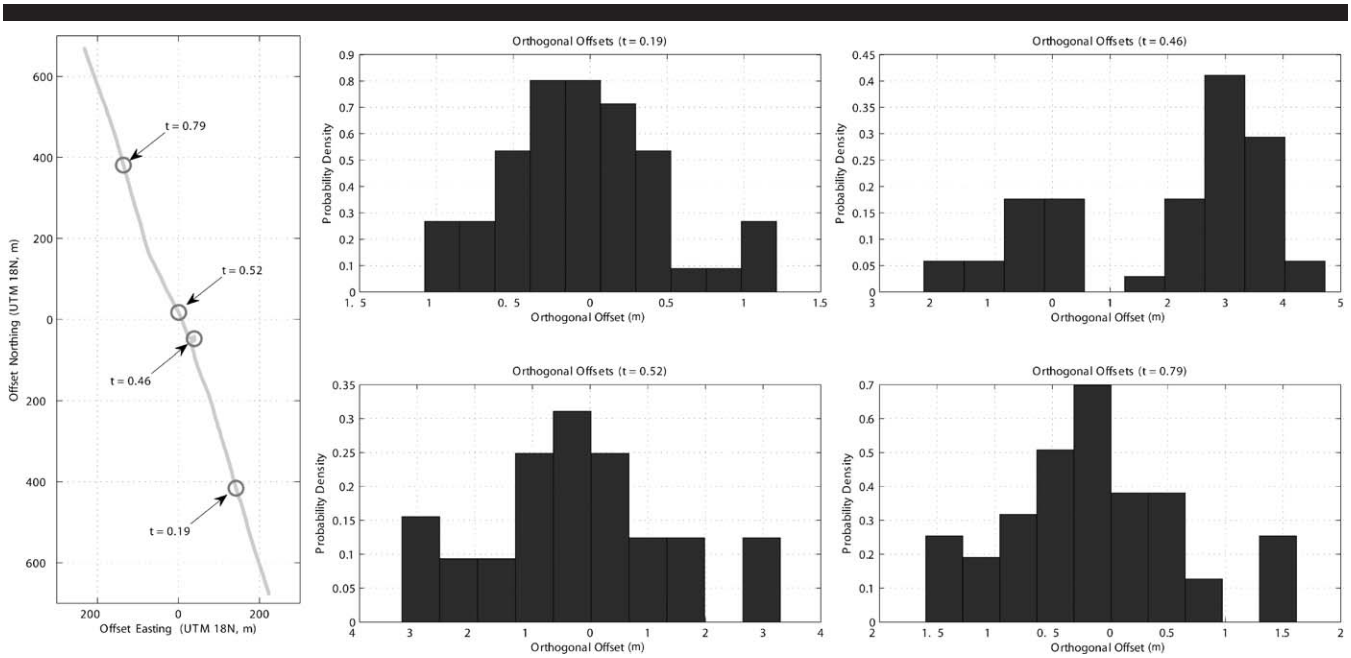

Figure 5. Examples of distribution of offsets within the ensemble along the reference shoreline. The probability density function estimates show mostly symmetrical distributions, occasionally with slightly higher than normal tails, but reflect the variation in uncertainty along the reference shoreline (*cf.* Figure 8). The distribution about the pier (top right panel) is clearly an outlier, as described in the text. The ability to examine statistics of the shoreline variability in detail like this is a significant advantage of the Monte Carlo technique.

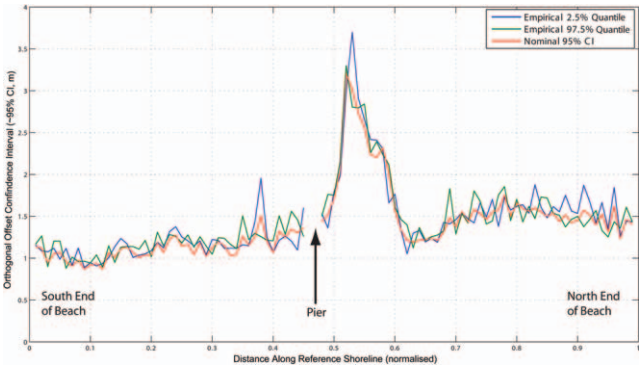

Figure 6. Estimates of horizontal uncertainty using theoretical (scaled standard deviation) and empirical (quantiles of the empirical cumulative density function) methods. Horizontal uncertainty is estimated to be approximately 1.0 m (95%) at the southern end of the shoreline (left), to rise to about 3.3 m (95%) immediately after the pier, and to return to about 1.5 m (95%) at the northern end (right). The small differences among the estimates suggest some small asymmetry of the distribution of offsets about the reference curve and some level of sampling noise due to the small size of the estimation ensemble.

tions or water level observations. Thus, we can satisfy two of the main criteria for a good empirical accuracy assessment: *i.e.,* that the reference ("truth") data be independent of and significantly more accurate than the data they are being used to test.

(3) By providing discrete reference points along the shoreline, the method enables accuracy to be computed following the Federal Geographic Data Committee's National Standard for Spatial Data Accuracy (NSSDA; FGDC, 1998).

The results further showed that, as long as the survey locations along each transect are kept reasonably close (~5 m in our study), the method is invariant to the interpolation strategy used to estimate the MHW zero-crossing location along each transect.

Our analysis of the Monte Carlo–based uncertainty assessment indicates that the results are consistent with those determined through the field campaign at Duck, showing uncertainties on the order of 1.0 to 1.5 m (95%) over much of the shoreline, with local increases to as much as 3.3 m (95%) in specific locations. Investigation of the beach slope across the shoreline in the test area indicates that local variation of slope can explain much of the variability in the uncertainty estimates, with higher uncertainties being evident in areas with smaller slope. (For the same vertical change in depths due to modeled errors in measurements, lower slope regions generate more significant horizontal changes in computed LIDAR-derived MHW shoreline.) The Monte Carlo analysis does not require, and is not provided with, any information on local slope, however, so we may conclude that the effects are physically derived rather than an artifact of any processing anomalies.

The fidelity of the uncertainty estimates produced using this method depends heavily on the quality of the uncertainty estimates for the raw measurements and to a lesser extent on the model used to generate the realizations. Our agreement, at least in the test case, with the ground-truth measurements suggests that our initial model is at least first-order accurate, although testing in other environments is required to verify that the results match the ground-truth measurements in general. Obtaining reliable estimates of the uncertainty of the raw measurements remains, to some extent, a difficult problem. The majority of the measurements can be obtained from manufacturers of auxiliary equipment (*e.g.,* for motion sensors), classical geodetic procedures (*e.g.,* accuracy of offsets among components in the survey system), and normal calibration procedures (*e.g.,* accuracy of alignment between the motion sensor and the scanner platforms). Some, however, require more detailed knowledge of the performance and construction of the scanner platform itself and are more difficult to obtain. While it is possible to approximate some of these features (as we have done here with the range measurement uncertainty), a more detailed, manufacturer-supplied model would be preferable; determining the significance of these effects so as to assess how much effort to invest in improving their accuracy is a subject of our ongoing research.

The Monte Carlo technique used in this example is relatively simple theoretically but is more costly computationally than more analytic procedures used to determine uncertainty. In practice, however, the number of steps and the nonlinear and algorithmic nature of the steps means that it would be extremely difficult, if not impossible, to predict analytically the uncertainty of the product shoreline (as opposed to the individual LIDAR measurements). Assessing the uncertainty with ground-truth measurements for each survey is also time consuming and clearly impractical. Whatever the cost, therefore, a simulation approach such as the one outlined here appears to be the only computationally tractable and practical method. The absolute computational cost remains important, but our tests indicate that even a simple implementation of the method in an interpreted language is relatively efficient, completing in under an hour for the sorts of datasets considered here without any attempt at optimization. (This also includes the geographic information system steps to model the shoreline extraction methodology.) The method is expected to be of $O(NM)$ complexity for N members of the ensemble and M test points along the reference shoreline, which is a reasonable computational burden on modern hardware.

A fundamental question of Monte Carlo analyses in general is the number of members, N, in the ensemble for a given level of accuracy in the estimates. Our tests here with $N \approx 50$ show some evidence of effects in the estimates that may be related to Monte Carlo estimation noise more than to the data themselves. Although we have not done so in this case, we expect that this could be readily addressed by increasing the number of samples in the ensemble, with relatively low computational cost increase. Methods for estimating the number of ensemble members exist but are complicated when the statistical properties of the estimates are unknown in general, as here. It is likely that the only way to determine the appropriate number is simply to try with larger numbers

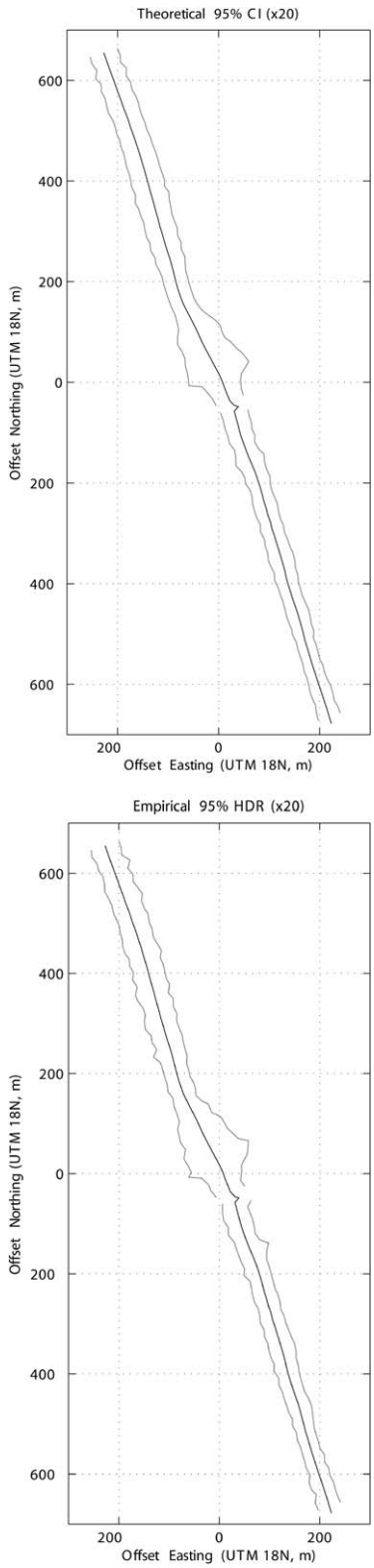

Figure 7. Reference shoreline outer 95% CI bounds as estimated using the Monte Carlo method and (top) a theoretical model of the CI based on an assumed distribution; (bottom) the empirical bounds computed from the data. The results are broadly similar (*cf.* Figure 6), and in both cases the offset of the boundary curves from the reference is exaggerated 20 times to make them visible at the scale of the whole shoreline.

of samples until the estimates settle within an allowable tolerance. This topic is also an aspect of our ongoing research.

The stability of the method relies on being able to determine an algorithmic as opposed to a subjective shoreline—in this case, the 0-m curve at MHW after appropriate geodetic transformations. The national shoreline, however, consists of many anthropogenic structures, in addition to the natural shoreline, which would not satisfy this requirement. (The pier region in the test case here is a particular example of this effect.) In practice, although it would be difficult to automatically detect these elements in unstructured data, they typically do not have their positions, or their contribution to the juridical shoreline, determined from such data. Rather, they are typically derived from aerial photogrammetry, which has distinctly different uncertainty properties and error sources. We have chosen not to attempt to increase the complexity of the method to accommodate such structures, preferring instead to consider the matter separately in further research. For our current purposes, an appropriate protocol would be to remove the elevations that are not considered part of the natural shoreline from the dataset before the Monte Carlo processing, thereby obviating the problem, and add the uncertainty of the anthropogenic structures to the analysis at a later stage.

CONCLUSIONS

In this paper, we presented two new approaches to assessing the positional uncertainty in NGS's LIDAR-derived national shoreline. The first method is an empirical approach using transects surveyed with a Topcon Laser-Zone integrated laser level and RTK GPS system. This method was shown to work well, providing reference (ground truth) data that are (1) highly accurate and (2) independent of the data they are being used to test. Furthermore, we found that the field methodology was invariant to the interpolation technique used to estimate the MHW zero-crossing location along each transect, provided that the distance between adjacent survey points is kept small, and to the method used to measure distances from the LIDAR-derived shoreline to the truth locations.

Despite these benefits of the new empirical approach, there are significant advantages to also developing empirically independent statistical methods of assessing the positional uncertainty in NGS's LIDAR-derived national shoreline. Specifically, the simulated statistical methods are needed to satisfy international hydrographic surveying standards, perform sensitivity analysis, inform policy decisions within NGS, and address the practical concern that it is simply not feasible to perform field surveys as part of every shoreline mapping project. To this end, the second method presented in this paper is a stochastic analysis, based on the Monte Carlo

method. Our approach entails generating an ensemble of shorelines resulting from different realizations of the random effects in the input measurements propagated through the entire shoreline mapping process. This ensemble of shoreline realizations can then be used to compute summary statistics describing the positional uncertainty in the LIDAR-derived shoreline.

In this study conducted using airborne LIDAR data and ground truth in the North Carolina Outer Banks, the Monte Carlo–based assessment of uncertainty showed similar estimates of horizontal uncertainty of the reference shoreline to the values determined by the ground-truth field program; our interpretation of the shoreline based on the two methods would at least be similar. This is encouraging, as it indicates that, in the future, NGS may be able to use the Monte Carlo approach operationally to assess the positional uncertainty in its shoreline without having to rely exclusively on expensive field surveys.

Assessment of the component uncertainties for the simulation model is tractable but remains the most difficult part of the analysis and the most likely to influence the outcome.

The method does not really treat objects that would be part of the shoreline but do not evince a zero-meter isobath: these are typically derived from another source in practice, however.

Further investigation is likely required to tune the size of the ensemble, details of the uncertainty models used, and assess the applicability of the method in other areas, and in the large. These are recommended topics for a proposed follow-on study.

LITERATURE CITED

ASPRS (American Society for Photogrammetry and Remote Sensing), 2009. LAS specification: version 1.3, R10. *Photogrammetric Engineering and Remote Sensing,* 75(9), 1035–1042.

Baltsavias, E.P., 1999. Airborne Laser Scanning: Basic Relations and Formulas. *ISPRS Journal of Photogrammetry & Remote Sensing,* (54)2–3, 199–214.

Boak, E.H. and Turner, I.L., 2005. Shoreline definition and detection: a review. *Journal of Coastal Research,* 21(4), 688–703.

Calder, B.R. and Mayer, L.A., 2003. Automatic processing of high-rate, high-density multibeam echosounder data. *Geochemistry, Geophysics, Geosystems,* 4(6), 1048, DOI 10.1029/2002GC000486.

Crowell, M.; Leatherman, S.P., and Buckley, M.E., 1991. Historical shoreline change: error analysis and mapping accuracy. *Journal of Coastal Research,* 7(3), 839–852.

FGDC (Federal Geographic Data Committee), 1998. Geospatial Positioning Accuracy Standards Part 3: National Standard for Spatial Data Accuracy. http://www.fgdc.gov/standards/projects/FGDC-standards-projects/accuracy/part3/chapter3. (accessed January 18, 2010).

Filin, S., 2001. Calibration of Airborne and Spaceborne Laser Altimeters Using Natural Surfaces. Columbus, Ohio: Ohio State University, Ph.D. thesis, 128p.

Graham, D.; Sault, M., and Bailey, J., 2003. National Ocean Service shoreline: past, present, and future. *In:* Byrnes, M.; Crowell, M., and Fowler, C. (eds.), *Shoreline Mapping and Change Analysis: Technical Considerations and Management Implications,* Journal of Coastal Research, Special Issue No. 38, pp. 14–32.

Habib, A.F.; Al-Durgham, M.; Kersting, A.P., and Quackenbush, P., 2008. Error budget of lidar systems and quality control of the derived point cloud. *In: Proceedings of the 21st International Society for Photogrammetry and Remote Sensing Congress, Commission I: Vol. 37, Part B* (Beijing, China).

Hare, R.; Godin, A., and Mayer, L.A., 1995. Accuracy Estimation of Canadian Swath (Multi-Beam) and Sweep (Multi-Transducer) Sounding Systems. Technical Report. Ottawa, Ontario, Canada: Canadian Hydrographic Service.

Hess, K.W., 2002. Spatial interpolation of tidal data in irregularly shaped coastal regions by numerical solution of Laplace's equation. *Estuarine, Coastal and Shelf Science,* 54(2), 175–192.

IHO (International Hydrographic Organization), 2008. *IHO Standards for Hydrographic Surveys,* 5th edition. Monaco: International Hydrographic Bureau, 36p.

Leatherman, S.P., 2003. Shoreline change mapping and management along the U.S. East Coast. *In:* Byrnes, M.; Crowell, M., and Fowler, C. (eds.), *Shoreline Mapping and Change Analysis: Technical Considerations and Management Implications,* Journal of Coastal Research, Special Issue No. 38, pp. 5–13.

Lindenberger, J., 1989. Test results of laser profiling for topographic terrain survey. *In: Proceedings of the 42nd Photogrammetric Week* (Stuttgart, Germany).

Liu, H.; Sherman, D., and Gu, S., 2007. Automated extraction of shorelines from airborne light detection and ranging data and accuracy assessment based on Monte Carlo simulation. *Journal of Coastal Research,* 23(6), 1359–1369.

Moore, L.J., 2000. Shoreline mapping techniques. *Journal of Coastal Research,* 16(1), 111–124.

Moore, L.J.; Ruggiero, P., and List, J.H., 2006. Comparing mean high water and high water line shorelines: should proxy-datum offsets be incorporated into shoreline change analysis? *Journal of Coastal Research,* 22(4), 894–905.

Morin, K.W., 2002. Calibration of Airborne Laser Scanners. Calgary, Alberta, Canada: University of Calgary, Master's thesis.

Morton, R.A., 1991. Accurate shoreline mapping: past, present, and future. *In:* Kraus, N.C.; Gingerich, K.J., and Kriebel, D.L. (eds.), *Coastal Sediments '91.* Seattle, Washington: American Society of Civil Engineers, pp. 997–1010.

Morton, R.A. and Speed, M.F., 1998. Evaluation of shorelines and legal boundaries controlled by water levels on sandy beaches. *Journal of Coastal Research,* 14(4), 1373–1384.

Morton, R.A.; Miller, T.L.; and Moore, L.J.; 2004. National Assessment of Shoreline Change: 1: Historical Shoreline Changes and Associated Coastal Land Loss along the U.S. Gulf of Mexico. U.S. Geological Survey Open-File Report 2004-1043, 45p.

Myers, E.; Hess, K.; Yang, Z.; Xu, J.; Wong, A.; Doyle, D.; Woolard, J.; White, S.; Le, B.; Gill, S., and Hovis, G., 2007. VDatum and strategies for national coverage. *In: Proceedings of the Marine Technology Society/IEEE OCEANS Conference* (Vancouver, British Columbia, Canada).

NOAA (National Oceanic and Atmospheric Administration), 2009. Estimation of Vertical Uncertainties in VDatum. http://vdatum.noaa.gov/download/publications/Estimation_Vertical_Uncertainties_VDatum.pdf (accessed January 18, 2010).

NRC (National Research Council), 2004. *A Geospatial Framework for the Coastal Zone: National Needs for Coastal Mapping and Charting*. Washington, D.C.: National Academy Press, 149p.

Pajak, M.J. and Leatherman, S.P., 2002. The high water line as shoreline indicator. *Journal of Coastal Research,* 18(2), 329–337.

Parker, B., 2002. The integration of bathymetry, topography and shoreline and the vertical datum transformations behind it. *International Hydrographic Review,* 3(3), 35–47.

Parrish, C., 2007. Vertical Object Extraction from Full-Waveform Lidar Data Using a 3D Wavelet-Based Approach. Madison: University of Wisconsin, Ph.D. thesis, 171p.

Parrish, C.E.; Sault, M.; White, S.A., and Sellars, J., 2005. Empirical analysis of aerial camera filters for shoreline mapping. *In: Proceedings of the American Society for Photogrammetry and Remote Sensing Annual Conference* (Baltimore, Maryland), unpaginated CD-ROM.

Press, W.H.; Teukolsky, S.A.; Vetterling, W.T. and Flannery, B.P., 1992. *Numerical Recipes in C: The Art of Scientific Computing,* 2nd edition. New York: Cambridge University Press, 994p.

Robertson, W.; Whitman, D.; Zhang, K., and Leatherman, S.P., 2004. Mapping shoreline position using airborne laser altimetry. *Journal of Coastal Research,* 20(3), 884–892.

Scavia, D.; Field, J.C.; Boesch, D.F.; Buddemeier, R.W.; Burkett, V.; Cayan, D.R.; Fogarty, M.; Harwell, M.A.; Howarth, R.W.; Mason, C.; Reed, D.J.; Royer, T.C.; Sallenger, A.H.; and Titus, J.G., 2002. Climate change impacts on U.S. coastal and marine ecosystems. *Estuaries and Coasts,* 25(2), 149–164.

Scott, G.; Wijekoon, N; and White, S., 2009. Multi-sensor mapping: integrating data streams for coastal science and management. *Hydro International,* 13(2), 20–23.

Shalowitz, A.L., 1964. *Shore and Sea Boundaries,*. Washington, DC: U.S. Department of Commerce, Coast and Geodetic Survey, U.S. Government Printing Office, 420p.

Smith, J.T., Jr., 1981. *A History of Flying and Photography in the Photogrammetry Division of the National Ocean Survey, 1919–79*. Silver Spring, Maryland: U.S. Department of Commerce, National Oceanic and Atmospheric Administration, National Ocean Service, 486p.

Snay, R.A. and Soler, T., 2008. Continuously operating reference stations (CORS): history, applications and future enhancements. *Journal of Survey Engineering,* 134(4), 95–104.

Stockdon, H.F.; Sallenger, A.H., Jr.; List, J.H., and Holman, R.A., 2002. Estimation of shoreline position and change using airborne topographic lidar data. *Journal of Coastal Research,* 18(3), 502–513.

Titus, J.G. and Richman, C., 2001. Maps of lands vulnerable to sea level rise: modeled elevations along the U.S. Atlantic and Gulf Coasts. *Climate Research,* 18(3), 205–228.

Vaughn, C.R.; Bufton, J.L.; Krabill, W.B., and Rabine, D., 1996. Georeferencing of airborne laser altimeter measurements. *International Journal of Remote Sensing,* 17(11), 2185–2200.

White, S., 2007. Utilization of LIDAR and NOAA's vertical datum transformation tool (VDatum) for shoreline delineation. *In: Proceedings of the Marine Technology Society/IEEE OCEANS Conference* (Vancouver, British Columbia).